

# Metastable states of ozone calculated on an accurate potential energy surface

Dmitri Babikov,<sup>a)</sup> Brian K. Kendrick, Robert B. Walker, and Russell T Pack  
*Theoretical Division (T-12, MS B268), Los Alamos National Laboratory, Los Alamos, New Mexico 87545*

Paul Fleurat-Lesard and Reinhard Schinke  
*Max-Planck-Institute für Strömungsforschung, D-37073 Göttingen, Germany*

(Received 30 December 2002; accepted 15 January 2003)

A new potential energy surface for ozone is developed. It is based on high level *ab initio* data and includes an accurate description of the barrier region. Full quantum reactive scattering calculations using a coupled channel approach and hyperspherical coordinates are performed on this surface for various isotopic compositions of ozone. Collision lifetimes are obtained over a wide energy range, which gives the spectrum of rovibrational metastable states (scattering resonances). This spectrum is discovered to be very nonstatistical. The spectrum of resonances is dense below the isotopic zero-point-energy threshold and sparse above it. This feature is explained by the opening of additional dissociation channels at higher energies. This behavior is a general quantum mechanical effect that should occur in other triatomic molecules. © 2003 American Institute of Physics.

[DOI: 10.1063/1.1557936]

## I. INTRODUCTION

Oxygen has three stable isotopes: <sup>16</sup>O, <sup>17</sup>O, and <sup>18</sup>O. The isotope <sup>16</sup>O is the most abundant in the atmosphere, so that most oxygen molecules (O<sub>2</sub>) only include <sup>16</sup>O atoms. However, it has been known for more than 20 years now that, as first reported<sup>1</sup> in 1981, stratospheric ozone (O<sub>3</sub>) shows strange, large enrichments in the heavy isotopes of oxygen relative to the oxygen from which it is formed. These anomalous enrichments were confirmed in 1983 by laboratory studies,<sup>2</sup> and, they were found to be “mass independent,” i.e., almost equal for <sup>17</sup>O and <sup>18</sup>O. For recent short reviews, see Thieme<sup>3</sup> and Mauersberger *et al.*<sup>4</sup>

Nowadays it is understood<sup>3–8</sup> that the recombination reaction which forms ozone



where the third body M can be any atmospheric atom or molecule, is responsible for the anomalous isotope effect in ozone formation. Its rate is unusually sensitive to the isotopic composition of the oxygen atoms involved; i.e., its rates can differ by more than 50% for different isotopic compositions, which is a remarkably large isotope effect! The rates do depend on masses; however, the dependence is very complex, so that no obvious correlation can be derived.

It has been accepted by most authors that at low pressure process (1) is dominated by the *energy transfer* (ET) mechanism



Here O<sub>3</sub><sup>\*</sup> is a rovibrational metastable state (or scattering resonance) which lives long enough to be stabilized by the

collision with M. Again, any combination of O isotopes can be involved. To calculate the reaction rate *via* (2) and (3) one must know, first, the energies, lifetimes, and rates of formation and dissociation of the metastable (O<sub>3</sub><sup>\*</sup>) states. Second, one must know the rates of the stabilization step (3) for different metastable states and isotopic combinations. All these are not yet available.

It has been also recognized,<sup>9–11</sup> that accurate detailed quantum mechanical calculations for various isotopic substitutions in reactions (2) and (3) are needed in order to accurately describe the isotope effects. Calculations of this kind,

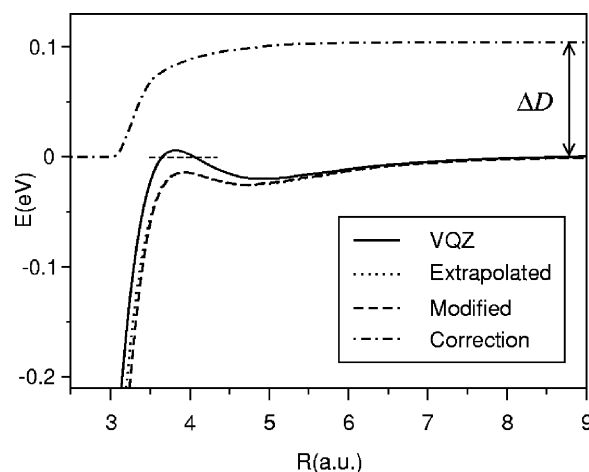


FIG. 1. One-dimensional cut of the potential energy surface for ozone along the minimum energy path for dissociation/recombination (O<sub>3</sub> ↔ O<sub>2</sub> + O). The horizontal axis gives the distance between the most distant end O atom and the central O atom. For the original cc-pVQZ surface the barrier above the dissociation limit is clearly seen. The barrier of the modified surface, constructed in the present work, is below the dissociation limit and is in good agreement with the data obtained by extrapolation to the infinite basis set limit. See text for details. The correction function along the minimum energy path is shown at the top. It provides the correction ΔD to the dissociation energy.

<sup>a)</sup>Author to whom correspondence should be addressed. Electronic mail: babikov@lanl.gov

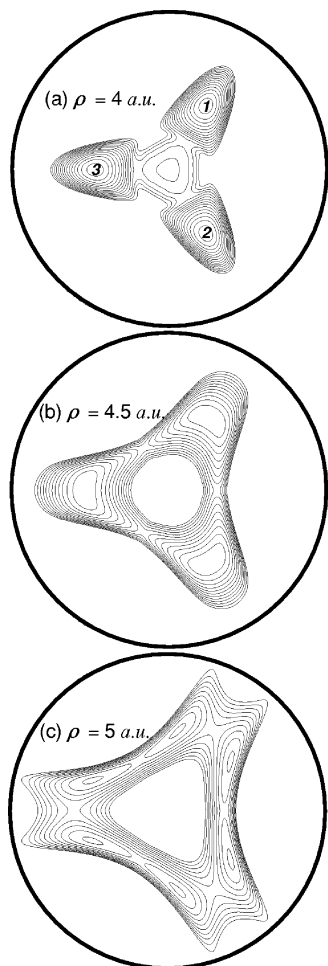


FIG. 2. Two-dimensional slices of the potential energy surface in hyperspherical coordinates at small values of hyperradius. The fixed value of the hyperradius  $\rho$  is given for each frame; two hyperangles are varied. Contours are spaced by 0.2 eV with the highest contour at 1.8 eV above the  $O_2+O$  dissociation limit which is taken as energy zero. (a)  $\rho=4$  a.u., the lowest contour is at  $-1.0$  eV. The three open minima of  $O_3$ , separated by large energy barriers, are clearly seen. (b)  $\rho=4.5$  a.u., the lowest contour is at  $-0.4$  eV. Increasing the hyperradius decreases the barriers between the minima. (c)  $\rho=5$  a.u., the lowest contour is at 0 eV. Permutation of nuclei in  $O_3$  is now possible.

especially for a molecule as complex as ozone, require state-of-the-art theory and computations. We have made an important step in this direction: The first full quantum mechanical calculations of the  $O_3^*$  rovibrational resonances on an accurate new potential energy surface for several isotopic compositions of the ozone:  $^{16}O^{18}O^{18}O$ ,  $^{18}O^{16}O^{16}O$ , and  $^{16}O^{16}O^{16}O$ . We have briefly reported some of our results in a recent Communication;<sup>12</sup> the present paper gives more details of the calculations. In Sec. II we discuss the potential energy surface (PES). In Sec. III we describe the method used for reactive scattering calculations. Results of these calculations are given and discussed in Sec. IV.

## II. POTENTIAL ENERGY SURFACE

In this work we discuss two potential energy surfaces. The first one is the original *ab initio* PES of Schinke and co-workers<sup>13</sup> (hereinafter referred to as “original”). The sec-

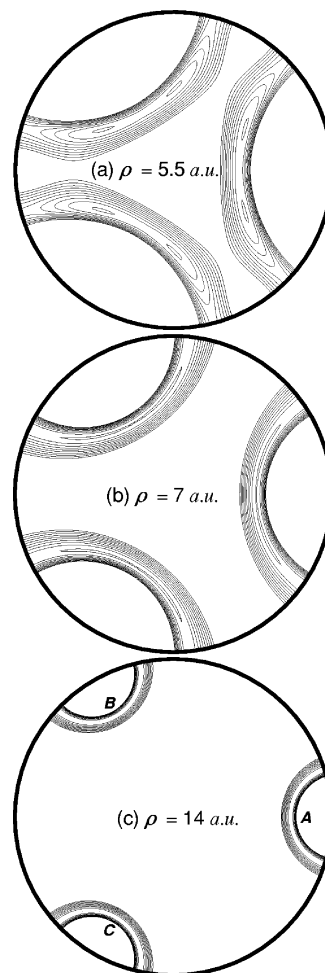


FIG. 3. Same as Fig. 2, but at large values of hyperradius. (a)  $\rho=5.5$  a.u., the lowest contour is at 0 eV. Formation of the asymptotic channels begins. (b)  $\rho=7$  a.u., the lowest contour is at 0 eV. Increasing the hyperradius separates the asymptotic channels. (c)  $\rho=14$  a.u., the lowest contour is at 0.2 eV. Three  $O_2+O$  dissociation channels are clearly seen.

ond surface (hereinafter referred to as “modified”) was constructed to address several problems with the original surface.

The original PES<sup>13</sup> is the best complete *ab initio* surface for ozone currently available in the literature. Calculations at the icMRCI+Q/cc-pVQZ level using a CASSCF(12,9) reference space were performed using the MOLPRO suite of *ab initio* programs. More than 5000 *ab initio* points were calculated and a three-dimensional cubic spline was constructed. Spectra for bound states of ozone were calculated using this surface and excellent agreement with experimental data was obtained.<sup>14</sup>

Though this original PES is the best that has been available for ozone, it has several problems. First of all, the dissociation energy of ozone ( $O_3 \rightarrow O_2 + O$ ) on the original surface is  $D_{VQZ}=1.027$  eV, which is about 10% smaller than the experimental value<sup>15</sup> of  $D_{EXP}=1.132 \pm 0.017$  eV. An increase of almost 10% in well depth is expected to result in many more high lying bound vibrational states and also increases the density of states near the dissociation limit. Having a correct number of states in this part of the spectrum is important for a describing the stabilization step (3) in the

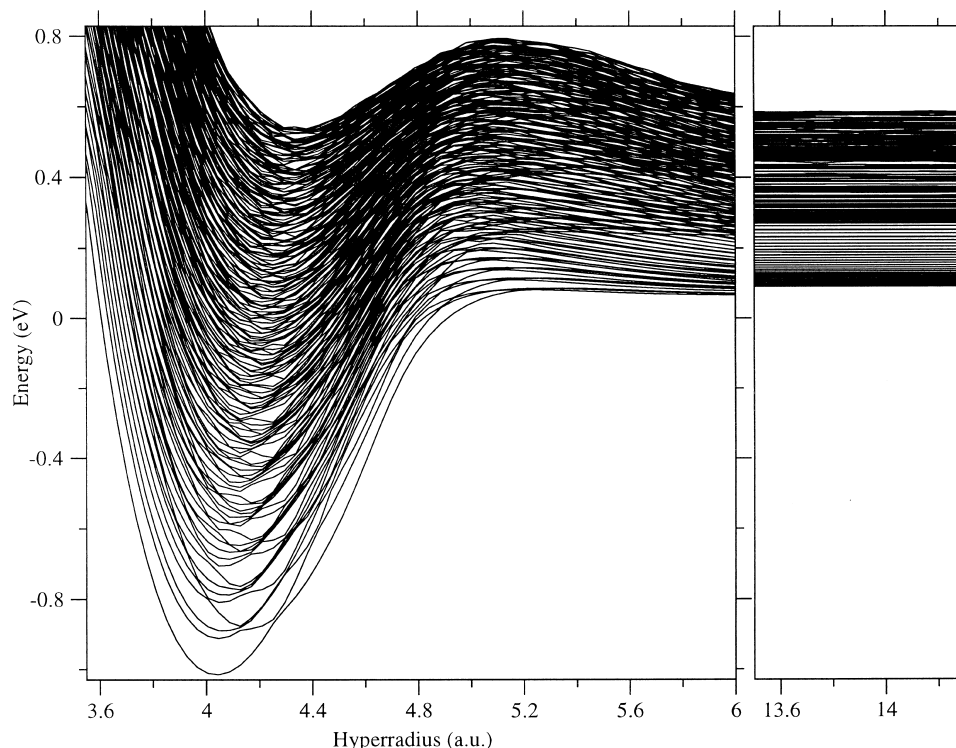


FIG. 4. Surface function energies vs hyperradius  $\rho$  for all 190 two-dimensional surface functions calculated for  $^{16}\text{O}^{18}\text{O}^{18}\text{O}$ . The left frame shows the well region. The right frame shows the asymptotic region. In the well region the surface function energies cover an energy range up to at least 0.55 eV above zero. In the asymptotic region the surface function energies are accurate up to 0.4 eV. These provide a very accurate basis set for the low energy scattering calculations performed in this work. See text for convergence data.

ozone formation, since stable  $\text{O}_3$  molecules are expected to be formed with energies very close to the dissociation limit.

The second problem of the original surface is its inaccurate behavior in the barrier region. Ozone is a bent triatomic ( $r_1 = r_2 \approx 2.4$  a.u.,  $\alpha \approx 117^\circ$ ); it dissociates by losing one end (terminal) O atom. The solid line in Fig. 1 shows a one dimensional cut of the original PES along the minimum energy path (MEP), as one end O atom leaves the molecule. The surface exhibits a small barrier of  $47 \text{ cm}^{-1}$  above the dissociation limit. After the original cc-pVQZ basis set calculations were done, two calculations with cc-pVTZ and cc-pV5Z basis sets were performed along the MEP,<sup>16,17</sup> and extrapolation to the infinite basis set limit were done.<sup>17</sup> The result of the extrapolation to the infinite basis set limit is shown on Fig. 1 as the dotted line, and the reader can see that although the general barrier shape and its location are similar to those of the original PES, the barrier height is quite different: it lies  $114 \text{ cm}^{-1}$  below the dissociation limit! So we conclude that the barrier of the original PES is an artifact. It has a drastic influence on the reaction dynamics at low collision energies, as has been shown by Fleurat-Lessard *et al.*<sup>17</sup> The positions and lifetimes of low-lying metastable states of ozone are also affected by this artifact, and, as we have shown elsewhere,<sup>12</sup> having the correct spectra of metastable states is crucial for the explanation of the anomalous rates of ozone formation.

To correct these problems we have built an additive analytic correction to the original surface:

$$V^{\text{modified}}(r_1, r_2, r_3) = V^{\text{original}}(r_1, r_2, r_3) + F^{\text{correction}}(r_2, r_3) - \Delta D.$$

Here  $\Delta D = D_{\text{EXP}} - D_{\text{VQZ}} = 0.105 \text{ eV}$  is the desired correction to the dissociation energy. The correction function is defined by the two longest bond distances of the  $\text{O}_3$  triatom ( $r_2$  and  $r_3$ , where  $r_1 < r_2 < r_3$ ) and switches smoothly between different dissociation channels,

$$F^{\text{correction}}(r_2, r_3) = \gamma P(r_2) + (1 - \gamma) P(r_3),$$

where

$$\gamma = \alpha - (\alpha - 1/2) \cdot \exp\{-\beta(r_3 - r_2)^2\}.$$

The one-dimensional correction component  $P(r)$  changes smoothly from zero at  $r'$  to  $\Delta D$  at  $r'''$

$$P(r) = \begin{cases} 0 & (r < r'), \\ \Delta D \cdot \frac{\sin\{f(r)\} + 1}{2} \cdot G(r) & (r' < r < r'''), \\ \Delta D & (r''' < r). \end{cases}$$

Here  $G(r)$  is used to slow down the growth of the function  $P(r)$  in the smaller  $r$  part of the correction interval

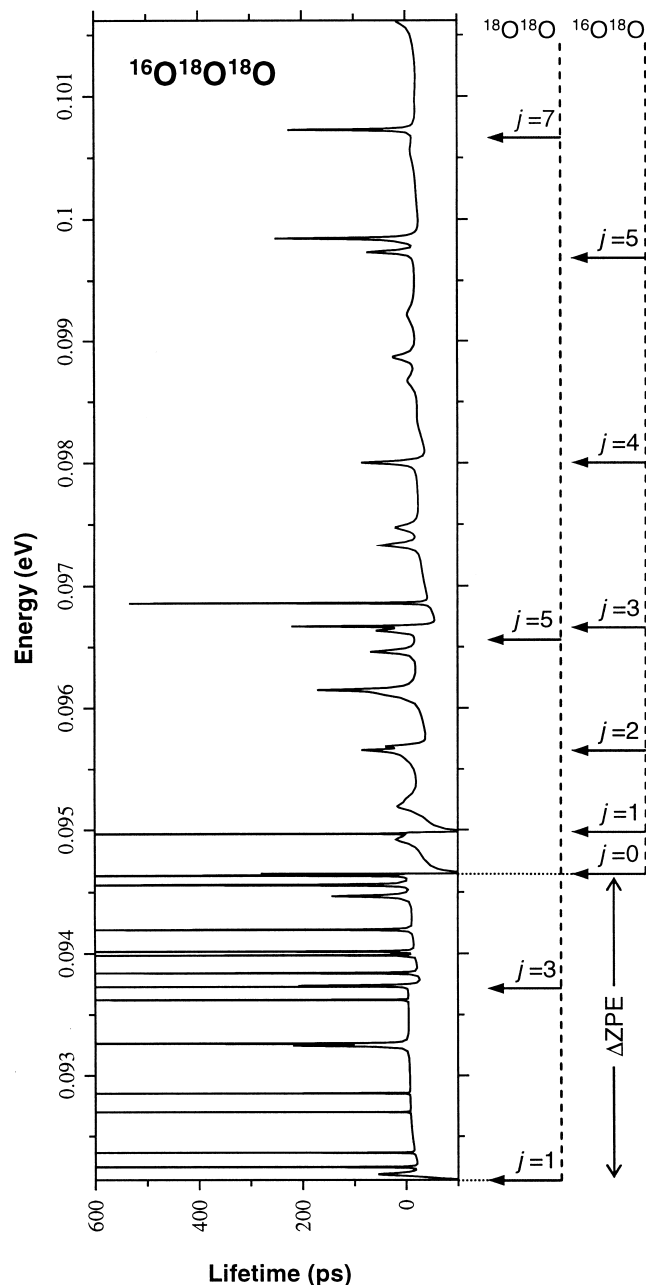


FIG. 5. Calculated lifetime spectra of metastable states for  $^{16}\text{O}^{18}\text{O}^{18}\text{O}$ . Sharp spikes to the left on the spectrum correspond to long-lived metastable states (scattering resonances). The asymptotic rotational states of  $^{18}\text{O}^{18}\text{O}$  and  $^{16}\text{O}^{18}\text{O}$  diatomics, as well as the  $\Delta\text{ZPE}$  energy range, are shown on the right. It is clearly seen that the  $\Delta\text{ZPE}$  part of the spectrum accommodates many long-lived metastable states, while the upper part of the spectrum is very sparse.

$$G(r) = \begin{cases} \frac{\sin\{f(r)\} + 1}{2} & (r' < r < r''), \\ 1 & (r'' < r < r'''). \end{cases}$$

Here  $r' < r'' < r'''$ . The function  $f(r)$  is given by:

$$f(r) = \log_c(ar + b),$$

with

$$a = (c^{\pi/2} - c^{-\pi/2}) / (r^{\text{end}} - r')$$

and

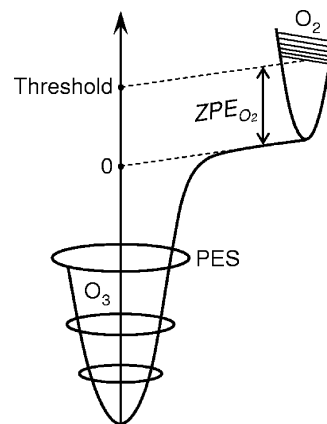


FIG. 6. Schematic of the potential energy surface. The energy zero is defined as the bottom of the dissociation channel. The scattering threshold occurs at the energy of the ground rovibrational state of  $\text{O}_2$  reactant, i.e., at its zero-point-energy ( $\text{ZPE}_{\text{O}_2}$ ).

$$b = c^{\pi/2} - ar^{\text{end}},$$

so that  $f(r)$  smoothly changes from  $-\pi/2$  at  $r'$  to  $\pi/2$  at  $r^{\text{end}}$  [ $r^{\text{end}} = r'''$  when  $f(r)$  is used in  $P(r)$ , and  $r^{\text{end}} = r''$  when  $f(r)$  is used in  $G(r)$ ].

In this procedure the points  $r'$ ,  $r''$ ,  $r'''$  and the parameter  $c$  are adjusted to fit the barrier shape obtained at the infinite basis set level (dotted curve in Fig. 1). The values  $r' = 4.5$  a.u.,  $r'' = 5.0$  a.u., and  $r''' = 8.0$  a.u. have been chosen. The value of  $c = 5.5$  has been chosen for  $f(r)$  when it is used in  $P(r)$ , and  $c = 1.5$  when  $f(r)$  is used in  $G(r)$ . The switching parameters are set to  $\alpha = 0$  and  $\beta = 30$ . The dash-dotted line in Fig. 1 shows a cut of  $F^{\text{correction}}(r_2, r_3)$  function along the MEP. The correction is zero near the global minimum (2.4 a.u.) and starts contributing only at 3.1 a.u., where the energy is already about 75% of the dissociation energy. It increases smoothly and at large distances (beyond 7 a.u.) it approaches a constant value, giving an energy shift equal to the dissociation energy change. A cut of the modified surface along the MEP is also shown in Fig. 1 as a dashed line and the reader can see that the barrier shape of the modified surface is in very good agreement with data extrapolated to the infinite basis set limit. (In Fig. 1 the dashed and dotted curves are almost indistinguishable in the barrier region and in the region of the van der Waals minimum; one can tell them apart only in the attractive region.)

By the construction of the correction function we have achieved the following goals:

- (1) The correction function is global, symmetric to interchange of three atoms, and smooth everywhere in three dimensions, so that the change introduced does not induce any unphysical behavior in the wave functions;
- (2) the correction affects only the upper part of the original surface, along the dissociation channels, where the wrong behavior in the barrier region was observed. The lower, most accurate part of the original surface remains unchanged;
- (3) the dissociation energy on the modified surface is increased by the correction and now matches the experimental value;

TABLE I. Positions and lifetimes of resonances at  $E < 110$  K for  $^{16}\text{O}^{18}\text{O}$ .

	Position of maximum (eV)	TrQ at the maximum (ps)	Approx. background (ps)	Lifetime (ps)
Below $\Delta ZPE$	0.092 185 842 919	54.87	-27.12	82.00
	0.092 244 614 178	1764.50	-22.61	1787.11
	0.092 363 172 710	5940.30	-16.76	5957.06
	0.092 696 312 078	37 204.59	-8.53	37 213.13
	0.092 851 921 238	22 651.25	-7.56	22 658.81
	0.093 246 889 569	218.40	-4.49	222.89
	0.093 263 111 860	1025.38	-4.49	1029.87
	0.093 621 618 760	15 969.84	-4.11	15 973.95
	0.093 729 058 313	142 853.45	-3.36	142 856.81
	0.093 737 992 752	208.86	-3.36	212.23
	0.093 840 679 815	734.87	-22.75	757.63
	0.093 985 099 738	3496.78	-17.24	3514.02
	0.094 017 262 367	1131.05	-16.20	1147.25
	0.094 192 793 343	880.46	-11.83	892.29
	0.094 466 682 735	144.24	-7.77	152.02
0.094 556 754 507	1150.44	-7.15	1157.58	
0.094 632 834 851	27 441.95	-6.32	27 448.27	
Above $\Delta ZPE$	0.094 923 881 122	18.99	-14.98	33.97
	0.094 968 368 504	3630.27	-12.21	3642.48
	0.095 190 240 080	16.74	-27.54	44.28
	0.095 656 511 870	86.85	-8.38	95.23
	0.095 684 360 620	41.05	-7.74	48.78
	0.096 146 746 540	171.43	-19.65	191.08
	0.096 460 577 175	69.99	-15.18	85.17
	0.096 633 110 750	58.12	-13.26	71.38
	0.096 669 178 601	222.06	-13.26	235.32
	0.096 860 167 374	536.33	-43.28	579.62
	0.097 331 280 754	46.64	-23.48	70.12
	0.097 472 239 173	20.33	-22.84	43.17
	0.098 002 535 592	86.27	-18.37	104.64
	0.098 674 941 270	-3.78	-19.01	15.23
	0.098 867 670 511	25.46	-17.73	43.19
	0.099 219 245 429	-3.17	-16.45	13.29
	0.099 731 734 333	76.58	-15.18	91.76
	0.099 843 539 404	252.74	-13.90	266.64
0.100 728 337 11	227.67	-17.09	244.76	
0.101 614 982 69	17.73	-14.54	32.27	

(4) the parameters of the correction function are chosen to fix the shape of the barrier region.

Finally, an isotropic van der Waals tail ( $\sim C_6/R^6$ ,  $C_6=30.26$  a.u.)<sup>18</sup> is smoothly attached to extend the surface from the edge of the original *ab initio* grid to infinite O+O<sub>2</sub> separations. Thus our modified PES is a very sophisticated surface and is the best currently available for the ground electronic state of the ozone molecule.

Several two-dimensional slices of the PES are shown in Figs. 2 and 3 as stereographic projections using symmetrized hyperspherical coordinates.<sup>19</sup> The slices correspond to constant values of the hyperradius  $\rho$ . At  $\rho=4.0$  a.u. [Fig. 2(a)] one sees three open minima of the ozone molecule, labeled as “1,” “2,” and “3;” they correspond to the three possible permutations of nuclei in the equilibrium (bent triatomic) configuration of O<sub>3</sub>. It is seen that once the ozone molecule is formed in one of the minima, a large energy is necessary to transfer it to another minimum, i.e., to exchange two atoms in the molecule. An energetically less expensive way of exchanging atoms is to stretch one O–O’O” bond to reach

$\rho \sim 5.0$  a.u. [see Fig. 2(c)], where one O atom can go around O’O” to reach an O’O”–O configuration, which correlates with another minimum. At  $\rho=14.0$  a.u. [Fig. 3(c)] one can clearly see three possible dissociation channels, labeled as “A,” “B,” and “C;” they correspond to three possible ways to form the O<sub>2</sub>+O products. Let us imagine that an O+O’O” collision starts asymptotically from channel A in Fig. 3(c). As the reagents approach, the hyperradius decreases [Fig. 3(b), to 3(a), to 2(c) and to 2(b)]. In the process of recombination an O atom can approach the O’O” diatomic from either side and form either OO’O” in minimum 1 or O’O”O in minimum 2 in Fig. 2(a), but the “choice” is made at  $\rho \sim 5.0$  a.u. [see Fig. 2(c)]. Similarly, the decay of OO’O” from minimum 1 in Fig. 2(a) proceeds through the increase of the hyperradius and gives either O+O’O” products in channel A or OO’+O” products in channel B in Fig. 3(c). Figures 2 and 3 clearly demonstrate that the hyperspherical formalism allows us to treat simultaneously and on the same footing, all possible permutations of the nuclei in the process of formation and decay of O<sub>3</sub>\* metastable states.

### III. REACTIVE SCATTERING CALCULATIONS

In this work we perform full quantum reactive scattering calculations in all six dimensions of the problem [ $3 \cdot (N - 1) = 6$  for  $N = 3$  atoms]. No approximations are made. Energies up to 0.052 eV ( $\approx 600$  K) above the dissociation threshold are studied. The present calculations are performed for total angular momentum  $J=0$ ; calculations for  $J>0$  are ongoing and will be reported later. A coupled channel (CC) approach using APH hyperspherical coordinates and a hybrid FBR/DVR<sup>20</sup> is employed. The parallel computer code of Kendrick<sup>21</sup> was used. Oxygen isotopes  $^{16}\text{O}$  and  $^{18}\text{O}$  are spinless bosons, so that the total wave function of  $\text{O}_3$  molecule (electronic multiplied by nuclear) must be symmetric with respect to exchange of two  $^{16}\text{O}$  or  $^{18}\text{O}$  atoms. The ground electronic state of  $\text{O}_3$  in the scattering  $\text{O}(^3P) + \text{O}_2(^3\Sigma_g^-)$  region,  $^1A'$ , is antisymmetric.<sup>22</sup> Thus, the nuclear wave function must also be antisymmetric, so that the product of electronic and nuclear wave functions is symmetric. To account for these symmetry restrictions a proper projection procedure and a choice of symmetric surface functions are performed as described in detail in Ref. 20 (for  $^{16}\text{O}^{18}\text{O}^{18}\text{O}$  and  $^{16}\text{O}^{16}\text{O}^{18}\text{O}$ ) and Ref. 23 (for  $^{16}\text{O}^{16}\text{O}^{16}\text{O}$ ).

The range of the hyperradius between 3.25 and 14.31 a.u. is subdivided into 150 sectors. Convergence studies show that as many as 190 channels are necessary. Calculation of the surface functions for one isotopic combination requires eight wall clock hours on one 16-processor node of the massively parallel supercomputer "Seaborg."<sup>24</sup> Figure 4 shows the surface function energies for  $^{16}\text{O}^{18}\text{O}^{18}\text{O}$ . The minimum of the lowest surface function energy occurs at  $\rho \sim 4.05$  a.u. and corresponds to the equilibrium configuration of ozone. In the region of the potential well ( $\rho \sim 4$  a.u.) the lowest surface function energy ( $E \sim -1.011$  eV) is converged to  $0.0026 \text{ cm}^{-1}$  and the highest ( $N=190$ ) surface function energy ( $E \sim 1.015$  eV) is converged to  $2.0 \text{ cm}^{-1}$ . In the asymptotic region ( $\rho \sim 14$  a.u.) the lowest surface function energy ( $E \sim 0.0908$ ) is converged to  $0.043 \text{ cm}^{-1}$  and the energy of surface function  $N=100$  ( $E \sim 0.38$  eV) is converged to  $2.2 \text{ cm}^{-1}$ .

Many adiabatic avoided crossings are seen in the well region ( $3.8 \text{ a.u.} < \rho < 4.4 \text{ a.u.}$ ). Though it is not easily seen on the scale of Fig. 4, the energy of the lowest surface function reflects the property of the modified PES barrier: it shows a small barrier at  $\rho \sim 5.2$  a.u., and its top is slightly below the dissociation threshold. In the asymptotic region of Fig. 4 ( $\rho > 14$  a.u.) the surface function energies are almost horizontal and correlate to the rovibrational states of  $\text{O}_2$  diatomics. Diatomic vibrational levels  $v=0$ ,  $v=1$ , and  $v=2$  are clearly seen, as well as the corresponding rotational structure. At energies considered in the present work, only the  $v=0$  ground vibrational states of the channel diatomics can be populated.

Propagation of the coupled channel equations is performed using the log-derivative method.<sup>25,26</sup> Propagation of 190 coupled channel equations for about 1400 values of scattering energy requires four wall clock hours on one 16-processor node of the massively parallel supercomputer "Seaborg."<sup>24</sup> Elements of the  $\mathbf{S}$ -matrix are initially labeled

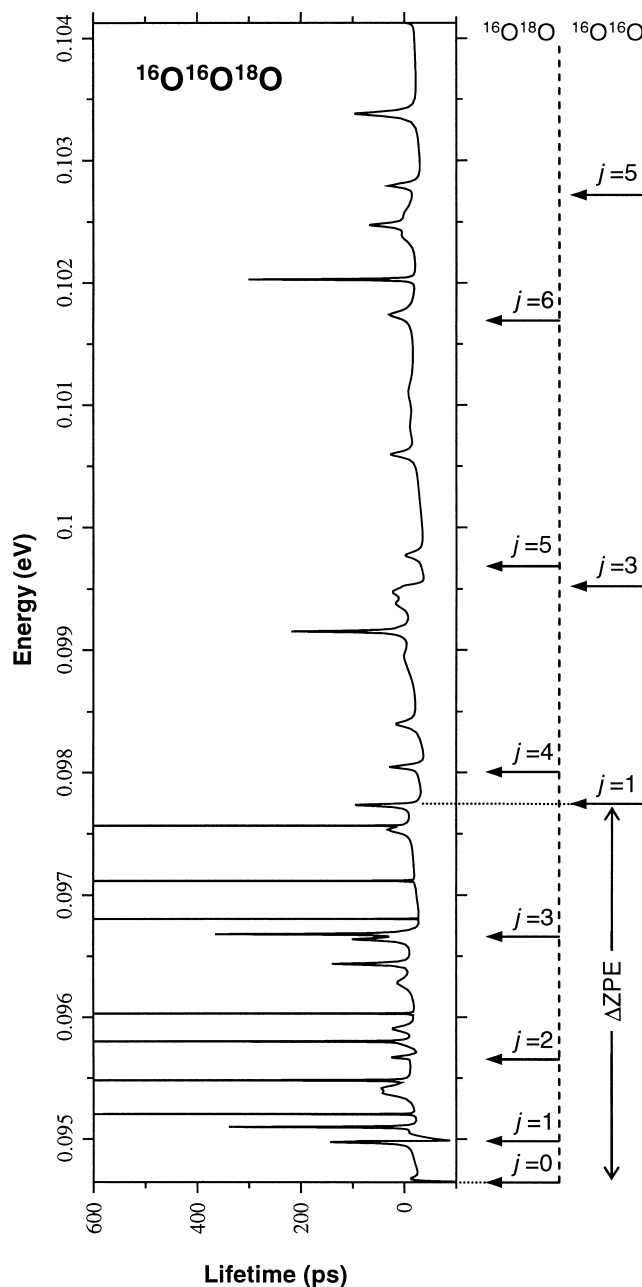


FIG. 7. Same as Fig. 5, but for  $^{16}\text{O}^{16}\text{O}^{18}\text{O}$ .

by arrangement channels. When two equivalent (experimentally indistinguishable) arrangement channels are present in ozone (let us say channels  $b$  and  $c$ ), then the  $\mathbf{S}$ -matrix contains several equivalent blocks

$$\mathbf{S} = \begin{pmatrix} S_{aa} & S_{ab} & S_{ac} \\ S_{ba} & S_{bb} & S_{bc} \\ S_{ca} & S_{cb} & S_{cc} \end{pmatrix},$$

where  $S_{ab} = S_{ac}$ ,  $S_{bb} = S_{cc}$ , etc. The physical  $\mathbf{S}$ -matrix describes the interference of these terms and is obtained according to the prescription of Zhang and Miller,<sup>27</sup> which in our case (*odd* rotational states of symmetric  $\text{O}_2$  diatomics, see Sec. IV) can be written as:

TABLE II. Positions and lifetimes of resonances at  $E < 110$  K for  $^{16}\text{O}^{16}\text{O}^{18}\text{O}$ .

	Position of maximum (eV)	TrQ at the maximum (ps)	Approx. background (ps)	Lifetime (ps)
Below $\Delta ZPE$	0.094 676 679 511	-11.01	-29.59	18.59
	0.094 973 588 219	143.51	-9.62	153.14
	0.095 098 011 781	339.28	-24.32	363.60
	0.095 203 220 593	2 575.48	-20.13	2 595.61
	0.095 378 524 211	42.66	-14.71	57.37
	0.095 414 001 232	44.59	-13.84	58.44
	0.095 480 260 653	882.28	-12.86	895.14
	0.095 669 895 552	25.35	-10.64	35.99
	0.095 800 394 724	981.41	-19.14	1 000.54
	0.095 903 645 314	24.09	-18.03	42.12
	0.096 030 058 735	4 024.95	-17.66	4 042.60
	0.096 283 149 739	14.10	-12.11	26.21
	0.096 436 903 430	139.60	-10.26	149.86
	0.096 638 156 661	101.21	-7.67	108.88
	0.096 680 636 260	365.27	-6.93	372.20
	0.096 805 313 511	17 397.71	-28.87	17 426.58
0.097 116 769 975	6 167.35	-20.02	6 187.37	
0.097 533 441 509	32.19	-11.42	43.61	
0.097 567 521 740	9 214.95	-10.98	9 225.94	
0.097 736 301 128	95.96	-8.72	104.68	
Above $\Delta ZPE$	0.098 046 334 509	28.97	-27.62	56.59
	0.098 397 717 036	17.48	-25.46	42.94
	0.098 948 259 629	1.08	-11.32	12.40
	0.099 151 073 591	218.06	-8.14	226.21
	0.099 380 542 911	17.10	-4.25	21.35
	0.099 474 685 043	23.84	-2.66	26.50
	0.099 773 678 034	-1.09	-28.20	27.11
	0.100 595 804 29	27.58	-19.11	46.69
	0.100 826 470 27	-10.38	-15.07	4.69
	0.101 104 422 86	-7.18	-12.18	5.00
	0.101 741 087 93	29.04	-15.64	44.67
	0.102 027 114 01	301.32	-19.96	321.28
	0.102 391 272 94	5.55	-16.07	21.62
	0.102 472 864 24	68.26	-15.64	83.90
	0.102 793 927 22	31.64	-18.67	50.30
	0.103 380 525 64	96.90	-21.70	118.60
0.104 148 484 37	170.95	-17.37	188.32	

$$\mathbf{S} = \begin{pmatrix} S_{aa} & \sqrt{2}S_{ab} \\ \sqrt{2}S_{ba} & S_{bb} - (-1)^j S_{bc} \end{pmatrix}.$$

When all three arrangement channels are experimentally indistinguishable the channel labeled  $\mathbf{S}$ -matrix has a form

$$\mathbf{S} = \begin{pmatrix} S_{aa} & S_{ab} & S_{ac} \\ S_{ba} & S_{bb} & S_{bc} \\ S_{ca} & S_{cb} & S_{cc} \end{pmatrix},$$

where  $S_{ab} = S_{ac} = S_{bc}$ ,  $S_{aa} = S_{bb} = S_{cc}$ , etc. In this case the physical  $\mathbf{S}$ -matrix (for *odd* rotational states of diatomics) is obtained as<sup>27</sup>

$$\mathbf{S} = (S_{aa} + 2S_{ab}).$$

The lifetimes of the metastable states<sup>23</sup> were obtained from the trace of Smith's  $\mathbf{Q}$ -matrix.<sup>28</sup>

#### IV. RESULTS

The structure of ozone is defined by the isotopes involved and their positions in the bent  $\text{O}_3$  triatomic. The first system we consider here consists of one  $^{16}\text{O}$  isotope and two  $^{18}\text{O}$  isotopes. They can form either an asymmetric  $^{16}\text{O}^{18}\text{O}^{18}\text{O}$  or a symmetric  $^{18}\text{O}^{16}\text{O}^{18}\text{O}$  molecule. The second system consists of one  $^{18}\text{O}$  isotope and two  $^{16}\text{O}$  isotopes; similarly, they can form either an asymmetric  $^{16}\text{O}^{16}\text{O}^{18}\text{O}$  or a symmetric  $^{16}\text{O}^{18}\text{O}^{16}\text{O}$  molecule. Hyperspherical coordinates allow us to treat all possible permutations of the nuclei simultaneously, so that both asymmetric and symmetric ozone isotopomers mentioned above are taken into account and the spectra of metastable states obtained describe all possible permutations of nuclei.

The low energy region (110 K above the threshold) of the calculated lifetime spectrum for  $(^{16}\text{O}^{18}\text{O}^{18}\text{O})^*$  is shown in Fig. 5. The lifetime obtained from Smith's  $\mathbf{Q}$ -matrix represents the difference between the actual time required for a collision and the time that a collision would have taken if the

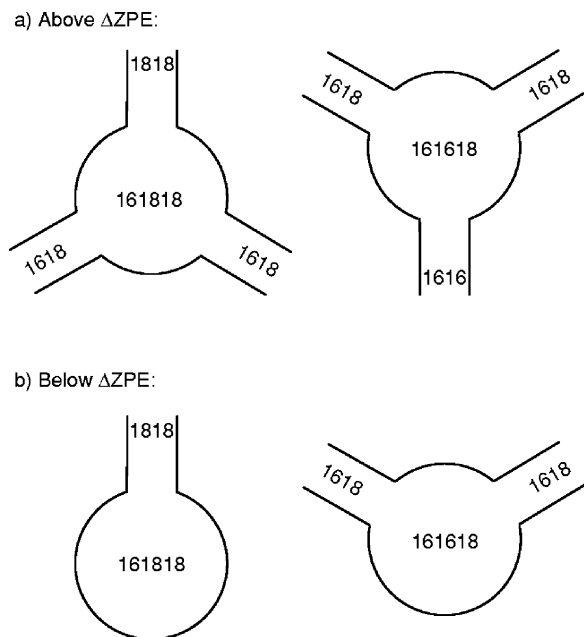


FIG. 8. Schematic for decay processes of the metastable states for  $^{16}\text{O}^{18}\text{O}$  and  $^{16}\text{O}^{16}\text{O}^{18}\text{O}$ . (a) At energies above the  $\Delta\text{ZPE}$  all three dissociation channels are open for both isotopic combinations and metastable states decay through three channels. (b) At energies below  $\Delta\text{ZPE}$  only one channel is open in the case of  $^{16}\text{O}^{18}\text{O}$  and two channels in the case of  $^{16}\text{O}^{16}\text{O}^{18}\text{O}$ . This increases the number of trapped molecules.

interaction potential were zero. Both the acceleration of reactants due to the strong attractive well and the shortened path due to the repulsive potential wall can make the actual collision time significantly shorter and thus lead to a negative background lifetime. Hence, the negative background of the spectrum corresponds to the relatively fast (nonresonant)  $\text{O}+\text{O}_2$  scattering or atom exchange processes, while the sharp spikes (scattering resonances) correspond to the formation of long-lived metastable  $\text{O}_3^*$  states.

The energy zero on Fig. 5 corresponds to the bottom of the entrance channel of the PES that describes free  $\text{O}+\text{O}_2$  reagents, i.e., to the bottom of the  $\text{O}_2$  potential curve. This is schematically depicted on Fig. 6. The threshold for formation of  $\text{O}_3^*$  (or  $\text{O}+\text{O}_2$ ) occurs when the total energy is high enough to form (in the entrance channel) a free diatomic  $\text{O}_2$

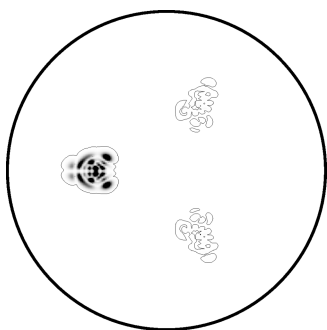


FIG. 9. A two-dimensional slice of the  $\text{O}_3^*$  wave function in hyperspherical coordinates. The value of the hyperradius is fixed at  $\rho=4$  a.u. as in Fig. 2(a). Darker colors correspond to higher probability density. One contour is shown at very small value (0.0001) to expose regions with a tiny probability density. See the text for discussion.

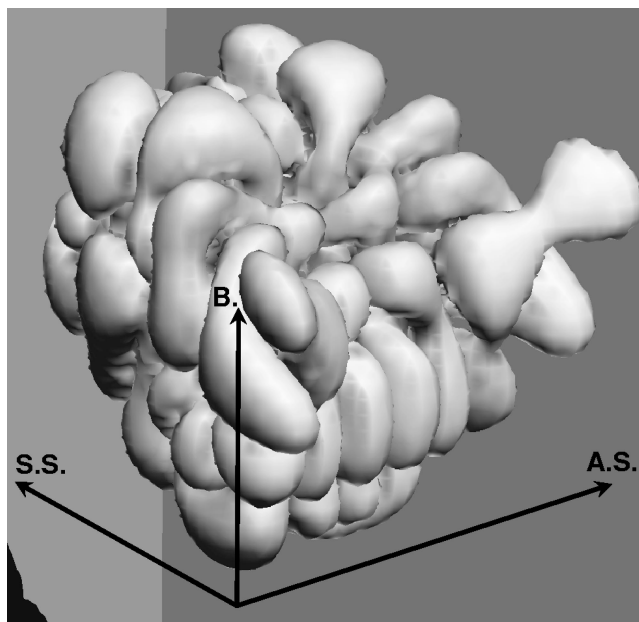


FIG. 10. Three-dimensional view of the  $\text{O}_3^*$  wave function in hyperspherical coordinates. The figure shows a range of the hyperradius  $3.74$  a.u.  $< \rho < 5.24$  a.u. that corresponds to the well region (see Fig. 4). The isosurface connects points in space with probability density equal to 0.01. See text for discussion.

in its ground rovibrational quantum state; thus the threshold energy is the zero-point energy (ZPE) of  $\text{O}_2$ . Energies below the scattering threshold correspond to the formation of bound quantum states of  $\text{O}_3$ . At the collision energies considered in this paper all  $\text{O}_2$  diatomics are in their ground vibrational state  $v=0$ . Both  $^{16}\text{O}$  and  $^{18}\text{O}$  are spinless bosons, so the total wave function (electronic multiplied by nuclear) of  $^{16}\text{O}^{16}\text{O}$  or  $^{18}\text{O}^{18}\text{O}$  must be symmetric with respect to nuclei exchange. The ground electronic state of  $\text{O}_2$ ,  $^3\Sigma_g^-$ , is antisymmetric. Thus, the nuclear wave function must also be antisymmetric so that the product of electronic and nuclear wave functions is symmetric. This fact restricts the quantum mechanical rotational states of  $^{16}\text{O}^{16}\text{O}$  and  $^{18}\text{O}^{18}\text{O}$  to the odd  $j$  manifold; i.e., they can occur only in odd rotational states ( $j=1, 3, 5, \dots$ ), while the asymmetric  $^{16}\text{O}^{18}\text{O}$  diatomic can occur in both even and odd rotational states ( $j=0, 1, 2, 3, \dots$ ).<sup>29</sup> The positions of the quantum rotational states for both  $^{18}\text{O}^{18}\text{O}$  and  $^{16}\text{O}^{18}\text{O}$  diatomics participating in the formation of  $(^{16}\text{O}^{18}\text{O})^*$  are also shown on Fig. 5. The threshold for metastable states corresponds, clearly, to the ground rovibrational state ( $v=0, j=1$ ) of the heavier diatomic  $^{18}\text{O}^{18}\text{O}$ . The corresponding energy is  $\text{ZPE}_{1818}=0.092140$  eV. The channel corresponding to the lighter diatomic  $^{16}\text{O}^{18}\text{O}$  opens at a slightly higher energy, which is the energy of its ground rovibrational state ( $v=0, j=0$ ):  $\text{ZPE}_{1618}=0.094648$  eV. The difference between these channels is  $\Delta\text{ZPE}=\text{ZPE}_{1618}-\text{ZPE}_{1818}=0.002508$  eV=29.1 K. One can see from Fig. 5 that opening of a new rotational channel sometimes causes some lowering of the lifetime; in the cases of  $^{18}\text{O}^{18}\text{O}$  ( $j=1$ ),  $^{16}\text{O}^{18}\text{O}$  ( $j=0$ ), and  $^{16}\text{O}^{18}\text{O}$  ( $j=1$ ) quite large negative dips are present in a spectrum.

The spectrum in Fig. 5 is very nonstatistical: The lower part of the spectrum ( $E<\Delta\text{ZPE}$ ) is dense—it contains *many*

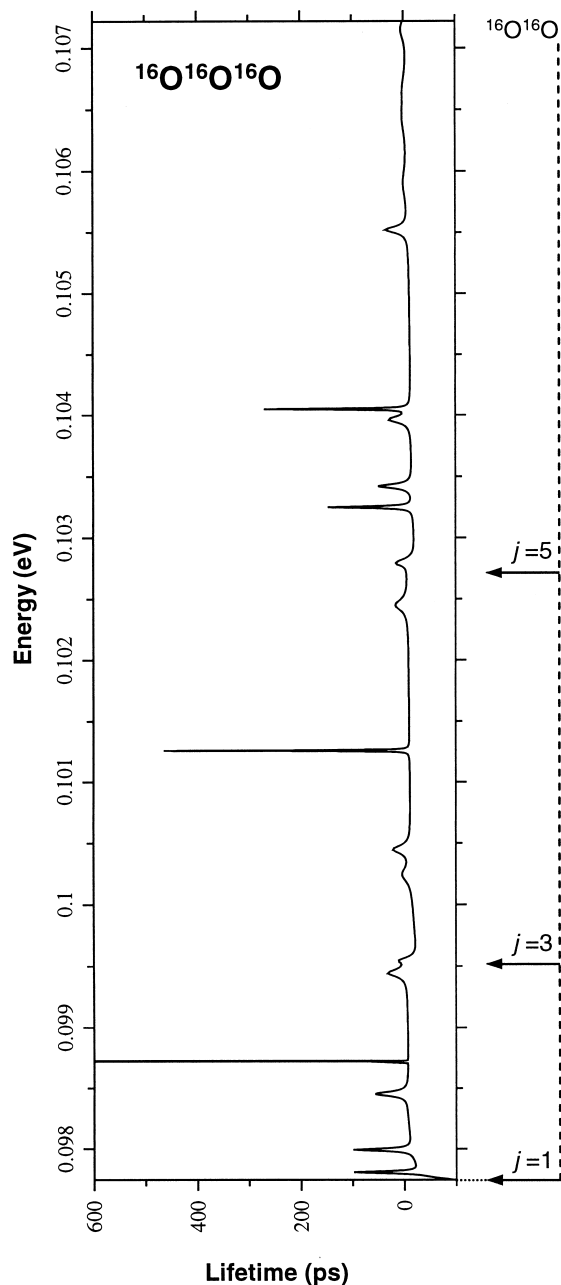


FIG. 11. Same as Fig. 5, but for  $^{16}\text{O}^{16}\text{O}^{16}\text{O}$ . Only a sparse spectrum is present.

*long-lived metastable states*, while the higher energy region of the spectrum is *very sparse* and contains only a few resonance features. Table I gives the positions and lifetimes of all the resonances shown on Fig. 5. Interpolation using a rational function was performed between calculated energy points in the vicinity of the resonance maximum and the positions and lifetimes of the interpolant maximum are given as the first and the second columns of the table. This procedure for locating the resonance maximum is very accurate. An approximate value of the negative nonresonant background in the region of each resonance is given in the third column. The total relative lifetime (value at the maximum minus the background value) is given in the last column. One can see that the part of the spectrum below  $\Delta\text{ZPE}$  accommodates 16

resonances with lifetimes above 100 ps, while the part above  $\Delta\text{ZPE}$  contains only seven such resonances.

Figure 7 shows the same part of the lifetime spectrum for the second isotopic composition ( $^{16}\text{O}^{16}\text{O}^{18}\text{O}$ )\*. In this case the heavier diatomic is  $^{16}\text{O}^{18}\text{O}$  and the threshold occurs at the energy of its ground rovibrational state ( $\nu=0, j=0$ ). The ground state ( $\nu=0, j=1$ ) of the lighter diatomic  $^{16}\text{O}^{16}\text{O}$  occurs at  $\text{ZPE}_{1616}=0.097\,745$  eV, so that in this case  $\Delta\text{ZPE} = \text{ZPE}_{1616} - \text{ZPE}_{1618} = 0.003\,097$  eV = 35.9 K. Again, a pronounced nonstatistical behavior is seen in the spectrum: the  $\Delta\text{ZPE}$  part of spectrum accommodates 13 resonances with lifetimes above 100 ps, while the upper part contains only four such resonances (see Table II).

Now let us try to understand the physical reason why the  $\Delta\text{ZPE}$  part of spectrum contains such a dense spectrum of long-lived metastable states. In the process (4) of formation/decay of the metastable states of  $\text{O}_3^*$ , there are three channels corresponding to the three possible permutations of O atoms taken to form the  $\text{O}_2$  diatomic. This is schematically depicted on Fig. 8. When a resonance state is formed at an energy above the  $\Delta\text{ZPE}$ , it can decay into any of three open channels. When a resonance is formed at an energy below the  $\Delta\text{ZPE}$ , it can decay only through one open channel in the case of  $^{16}\text{O}^{18}\text{O}^{18}\text{O}$ , or through two open channels in the case of  $^{16}\text{O}^{16}\text{O}^{18}\text{O}$ . Thus, resonance states formed below  $\Delta\text{ZPE}$  have fewer pathways to decay, and it is more so in the case of  $^{16}\text{O}^{18}\text{O}^{18}\text{O}$ . One should expect molecules to get trapped more often when there are fewer escape routes. This qualitatively explains why so many long-lived resonances occur below  $\Delta\text{ZPE}$ , and it also explains why the resonances are more dense in the case of  $^{16}\text{O}^{18}\text{O}^{18}\text{O}$  than in the case of  $^{16}\text{O}^{16}\text{O}^{18}\text{O}$ .

More constraints, specific to the ozone molecule, are imposed by the fact that the ozone molecule is a bent triatomic and dissociates more easily by releasing one of its end atoms, while dissociation of the central atom is energetically much more difficult. Insight into this process can be obtained by analyzing the metastable state wave functions. Here we show a wave function for the sharpest metastable state in the  $\Delta\text{ZPE}$  energy range for an ozone composed of one  $^{16}\text{O}$  atom and two  $^{18}\text{O}$  atoms. (The structure of this wave function is typical of the other long-lived metastable states in this energy region.) For this isotopic combination the two possible asymmetric isotopomers  $^{16}\text{O}^{18}\text{O}^{18}\text{O}$  are formed in minima “1” and “2” of the PES, while the symmetric isotopomer  $^{18}\text{O}^{16}\text{O}^{18}\text{O}$  is formed in minimum “3” [see Fig. 2(a)]. A two-dimensional slice of the wave function at  $\rho=4$  a.u. is shown in Fig. 9 [compare with Fig. 2(a)]. It is clearly seen that most of the probability is located in the  $^{18}\text{O}^{16}\text{O}^{18}\text{O}$  minimum and only small amounts of probability correspond to  $^{16}\text{O}^{18}\text{O}^{18}\text{O}$ . This behavior of the wave function suggests that the long lived metastable states within the  $\Delta\text{ZPE}$  energy range are trapped in the  $^{18}\text{O}^{16}\text{O}^{18}\text{O}$  minimum. Two possible channels for easy decay of such states ( $^{18}\text{O}^{16}\text{O}^{18}\text{O} \rightarrow ^{18}\text{O}^{16}\text{O} + ^{18}\text{O}$  and  $^{18}\text{O}^{16}\text{O}^{18}\text{O} \rightarrow ^{18}\text{O} + ^{16}\text{O}^{18}\text{O}$ ) are closed at these energies and decay proceeds by extraction only ( $^{18}\text{O}^{16}\text{O}^{18}\text{O} \rightarrow ^{16}\text{O} + ^{18}\text{O}^{18}\text{O}$ ), i.e., it is difficult. In contrast, decay from the two  $^{16}\text{O}^{18}\text{O}^{18}\text{O}$  minima is easy even at energies within the  $\Delta\text{ZPE}$  energy range ( $^{16}\text{O}^{18}\text{O}^{18}\text{O} \rightarrow ^{16}\text{O} + ^{18}\text{O}^{18}\text{O}$ ).

TABLE III. Positions and lifetimes of resonances at  $E < 110$  K for  $^{16}\text{O}^{16}\text{O}^{16}\text{O}$ .

Position of maximum (eV)	TrQ at the maximum (ps)	Approx. background (ps)	Lifetime (ps)
0.978 075 422 85E-01	98.22	-32.04	130.26
0.979 930 656 91E-01	99.02	-13.21	112.23
0.984 546 487 52E-01	57.56	-6.28	63.84
0.987 224 632 48E-01	14 267.10	-6.56	14 273.67
0.994 435 324 73E-01	31.77	-4.07	35.84
0.995 415 339 68E-01	11.48	-4.07	15.55
0.100 245 030 21	4.02	-13.09	17.12
0.100 446 976 67	21.45	-12.33	33.78
0.101 258 863 96	464.69	-10.24	474.93
0.102 450 441 47	16.49	-7.39	23.88
0.102 793 141 46	15.07	-6.63	21.70
0.103 247 980 24	146.49	-17.13	163.62
0.103 420 471 59	49.46	-15.87	65.33
0.103 963 456 56	28.94	-13.33	42.27
0.104 048 800 68	269.48	-13.17	282.65
0.105 520 371 06	34.69	-9.14	43.83
0.105 902 591 72	0.58	-8.42	9.01
0.106 450 460 00	2.64	-7.65	10.29
0.106 631 306 16	2.31	-7.43	9.75
0.107 151 242 75	5.22	-6.66	11.88

Figure 10 shows a three-dimensional view of the important part of this wave function (around minimum “3”) in the well region ( $3.74 \text{ a.u.} < \rho < 5.24 \text{ a.u.}$ , see Fig. 4). The three axes approximately describe symmetric stretch (S.S.), asymmetric stretch (A.S.) and bend (B.) motions of  $^{18}\text{O}^{16}\text{O}^{18}\text{O}$  triatomic. From the nodal structure, one can see that there is no preferred motion: The number of nodes in each direction is approximately the same and the wave function occupies approximately a spherical volume in space. The nodal structure is so dense and complex that we have not attempted to assign the normal mode quantum numbers to this wave function.

To further clarify the nonstatistical behavior of lifetime spectra for  $^{16}\text{O}^{18}\text{O}^{18}\text{O}$  and  $^{16}\text{O}^{16}\text{O}^{18}\text{O}$  we calculated the spectrum of metastable states for  $^{16}\text{O}^{16}\text{O}^{16}\text{O}$ , where there is no ZPE (due to symmetry) and all three fragmentation channels are open at all energies above the scattering threshold, as in Fig. 8(a). The resulting spectrum for  $^{16}\text{O}^{16}\text{O}^{16}\text{O}$  is shown in Fig. 11, and the positions and lifetimes of the resonances are given in Table III. One clearly sees that this spectrum contains a sparse part only, similar to those above the ZPE on Figs. 5 and 7. In the energy region  $E < 110$  K there are only seven resonances with lifetimes above 100 ps.

Finally, we recall that the original PES had a small barrier along the MEP:  $47 \text{ cm}^{-1} \approx 68 \text{ K}$  above the dissociation limit (see Fig. 1). Although small, this barrier is still twice as high as the narrow  $\Delta\text{ZPE}$  part of spectrum ( $\Delta\text{ZPE} = 29 \text{ K}$  for  $^{16}\text{O}^{18}\text{O}^{18}\text{O}$  and  $\Delta\text{ZPE} = 36 \text{ K}$  for  $^{16}\text{O}^{16}\text{O}^{18}\text{O}$ ). If such a barrier were present, it would prevent efficient population of the resonances in the  $\Delta\text{ZPE}$  part of spectrum. This fact reinforces the importance of correcting the original PES so that its behavior agrees with accurate *ab initio* calculations along the MEP (see Fig. 1). All the calculations described here have used the corrected modified PES.

## V. CONCLUSIONS

Full quantum reactive scattering calculations in a hyperspherical formulation have been carried out for  $\text{O} + \text{O}_2$  collisions. A sophisticated new *ab initio* potential energy surface has been used which includes an accurate representation of the barrier region along the MEP to dissociation. Lifetime spectra of metastable rovibrational  $\text{O}_3^*$  states have been obtained for three isotopic compositions:  $^{16}\text{O}^{18}\text{O}^{18}\text{O}$ ,  $^{16}\text{O}^{16}\text{O}^{18}\text{O}$ , and  $^{16}\text{O}^{16}\text{O}^{16}\text{O}$ . It is found that the lifetime spectra of the metastable states of  $^{16}\text{O}^{18}\text{O}^{18}\text{O}$  and  $^{16}\text{O}^{16}\text{O}^{18}\text{O}$  exhibit a pronounced nonstatistical feature: There are many long-lived metastable states within the narrow  $\Delta\text{ZPE}$  energy range, and there are only few metastable states at energies above the  $\Delta\text{ZPE}$  and their lifetimes are smaller. An explanation has been offered that this occurs because all possible dissociation channels are open at energies above the  $\Delta\text{ZPE}$ , while some of them are closed at energies below  $\Delta\text{ZPE}$ . In the case of  $^{16}\text{O}^{16}\text{O}^{16}\text{O}$ , when there is no  $\Delta\text{ZPE}$  and all three channels are always open, the spectrum of metastable states is sparse. We suggest that this property of metastable states is very general and should be seen in many other systems, where the interplay between the quantum zero-point-energies in different dissociation channels can produce a situation in which some arrangement channels are open while others are closed at the same scattering energy.

In a recent communication<sup>12</sup> we have demonstrated that this feature of the metastable states shows why there are anomalous isotope effects in the ozone formation rates. Full consideration of this topic will be given in a future publication.<sup>30</sup>

## ACKNOWLEDGMENTS

This work was performed under the auspices of the U.S. Department of Energy (under contract W-7405-ENG-36).

Dmitri Babikov acknowledges the Laboratory Directed Research and Development program at Los Alamos for granting a Postdoctoral Fellowship and the NERSC center at Lawrence Berkeley National Laboratory for computing support. The authors acknowledge Professor Konrad Mauersberger and his group at Heidelberg for helpful discussions on the anomalous isotope effect in ozone formation.

- <sup>1</sup>K. Mauersberger, *Geophys. Res. Lett.* **8**, 935 (1981).
- <sup>2</sup>M. H. Thiemens and J. E. Heidenreich III, *Science* **219**, 1073 (1983).
- <sup>3</sup>M. H. Thiemens, *Science* **283**, 341 (1999).
- <sup>4</sup>K. Mauersberger, B. Erbacher, D. Krankowsky, J. Gunther, and R. Nickel, *Science* **283**, 370 (1999).
- <sup>5</sup>S. M. Anderson, D. Hulsebusch, and K. Mauersberger, *J. Chem. Phys.* **107**, 5385 (1997).
- <sup>6</sup>C. Janssen, J. Guenther, D. Krankowsky, and K. Mauersberger, *J. Chem. Phys.* **111**, 7179 (1999).
- <sup>7</sup>D. Krankowsky and K. Mauersberger, *Science* **274**, 1324 (1996).
- <sup>8</sup>S. Wolf, M. Bitter, D. Krankowsky, and K. Mauersberger, *J. Chem. Phys.* **113**, 2684 (2000).
- <sup>9</sup>C. Janssen and R. A. Marcus, *Science* **294**, 951a (2001).
- <sup>10</sup>Y. Q. Gao and R. A. Marcus, *J. Chem. Phys.* **116**, 137 (2002).
- <sup>11</sup>C. Janssen, J. Guenther, K. Mauersberger, and D. Krankowsky, *Phys. Chem. Chem. Phys.* **3**, 4718 (2001).
- <sup>12</sup>D. Babikov, B. K. Kendrick, R. B. Walker, R. Schinke, and R. T Pack, *Chem. Phys. Lett.* (to be published).
- <sup>13</sup>R. Siebert, R. Schinke, and M. Bittererova, *Phys. Chem. Chem. Phys.* **3**, 1795 (2001).
- <sup>14</sup>R. Siebert, P. Fleurat-Lessard, M. Bittererova, S. C. Farantos, and R. Schinke, *J. Chem. Phys.* **116**, 9749 (2002).
- <sup>15</sup>M. W. Chase, Jr., C. A. Davies, J. R. Downey, Jr., D. J. Frurip, R. A. McDonald, and A. N. Syverud, *J. Phys. Chem. Ref. Data Suppl.* **14**, 1 (1985).
- <sup>16</sup>R. Hernandez-Lamonedada, M. R. Salazar, R. T Pack, *Chem. Phys. Lett.* **355**, 478 (2002).
- <sup>17</sup>P. Fleurat-Lessard, S. Yu. Grebenshchikov, R. Siebert, R. Schinke, and N. Halberstadt, *J. Chem. Phys.* **118**, 610 (2003).
- <sup>18</sup>D. J. Margoliash and W. J. Meath, *J. Chem. Phys.* **68**, 1426 (1978).
- <sup>19</sup>R. T Pack, and G. A. Parker, *J. Chem. Phys.* **87**, 3888 (1987).
- <sup>20</sup>B. K. Kendrick, R. T Pack, and R. B. Walker, *J. Chem. Phys.* **110**, 6673 (1999), and references therein.
- <sup>21</sup>B. K. Kendrick, *J. Chem. Phys.* **114**, 8796 (2001).
- <sup>22</sup>G. J. Atchity and K. Ruedenberg, *Theor. Chem. Acc.* **96**, 176 (1997).
- <sup>23</sup>B. Kendrick and R. T Pack, *J. Chem. Phys.* **106**, 3519 (1997).
- <sup>24</sup>IBM RS/6000 SP at NERSC center in Berkeley National Lab.
- <sup>25</sup>B. R. Johnson, *J. Chem. Phys.* **67**, 4086 (1977).
- <sup>26</sup>F. Mrugala and D. Secrest, *J. Chem. Phys.* **79**, 5960 (1983).
- <sup>27</sup>J. Z. H. Zhang and W. H. Miller, *J. Chem. Phys.* **91**, 1528 (1989).
- <sup>28</sup>F. T. Smith, *Phys. Rev.* **118**, 349 (1960).
- <sup>29</sup>G. Herzberg, *Molecular Spectra and Molecular Structure: I. Spectra of Diatomic Molecules*, 2nd ed. (Van Nostrand Reinhold, New York, 1950), Chap. III, p. 132.
- <sup>30</sup>D. Babikov, B. K. Kendrick, R. B. Walker, and R. T Pack (unpublished).